J Mol Model (2012) 18:3577–3586
DOI 10.1007/s00894-012-1362-y

ORIGINAL PAPER

Theoretical studies on all-metal binuclear sandwich-like complexes $M_2(\eta^4\text{-}E_4)_2$ (M=Al, Ga, In; E=Sb, Bi)

Congzhi Wang · Xiuhui Zhang · Jian Lu · Qianshu Li

Received: 30 October 2011 / Accepted: 10 January 2012 / Published online: 16 February 2012

Abstract A series of all-metal binuclear sandwich-like complexes with the formula $M_2(\eta^4\text{-}E_4)_2$ (M=Al, Ga, In; E=Sb, Bi) was studied by density functional theory (DFT). The most stable conformer for each of the $M_2(\eta^4\text{-}E_4)_2$ species is the staggered one with D_{4d} symmetry. The centred metal–metal bond in each $M_2(\eta^4\text{-}E_4)_2$ species is a covalent single bond, with the main contributors to these covalent bonds being the a_1 and e orbitals. For all these species, the interactions between the centred metal atoms and the all-metal ligands are covalent; $\eta^4\text{-}Sb_4^{2-}$ has a stronger ability to stabilize metal–metal bonds than $\eta^4\text{-}Bi_4^{2-}$. Nucleus-independent chemical shifts (NICS) values and molecular orbital (MO) analysis reveal that the all-metal $\eta^4\text{-}Sb_4^{2-}$ and $\eta^4\text{-}Bi_4^{2-}$ ligands in $M_2(\eta^4\text{-}E_4)_2$ possess conflicting aromaticity (σ antiaromaticity and π aromaticity), which differs from the all-metal multiple aromatic unit Al_4^{2-}. In addition, all of these $M_2(\eta^4\text{-}E_4)_2$ species are stable according to the dissociation energies of $M_2(\eta^4\text{-}E_4)_2 \rightarrow 2\ M(\eta^4\text{-}E_4)$ and $M_2(\eta^4\text{-}E_4)_2 \rightarrow 2\ M+2E_4$, and these stable species can be synthesized by two-step substitution reactions: $CpZnZnCp+2E_4^{2-} \rightarrow [E_4ZnZnE_4]^{2-}+2Cp^-$ and $[E_4ZnZnE_4]^{2-}+2\ M_2^+ \rightarrow E_4MME_4+2Zn^+$.

Keywords All-metal · Binuclear sandwich-like · Conflicting aromaticity · Density functional theory

C. Wang · X. Zhang (✉) · J. Lu · Q. Li (✉)
Institute of Chemical Physics, Beijing Institute of Technology, Beijing 100081, People's Republic of China
e-mail: zhangxiuhui@bit.edu.cn
e-mail: qsli@bit.edu.cn

Q. Li
Center for Computational Quantum Chemistry, South China Normal University, Guangzhou 510631, People's Republic of China

Introduction

Since the discovery of ferrocene [1], mononuclear sandwich-like complexes with cyclopentadienyl groups have received much attention in organometallic chemistry [2–7]. In 2004, the first stable binuclear metallocene Cp*ZnZnCp* (Cp*=C_5Me_5; Me=CH_3), in which the Zn atoms are formally in the +1 oxidation state in contrast to the common oxidation state +2 in its normal stable compound, was synthesized successfully [8]. This remarkable achievement opened up a new field in organometallic chemistry and triggered the interest of many groups in studying this kind of binuclear metallocenes [9, 10]. Recently, researchers found that binuclear sandwich-like complexes can be used in many areas of chemistry, such as catalysts, building blocks and potential hydrogen storage materials [11–13]. In metallocene chemistry, although the versatility of cyclopentadienyl groups or substituents has led to a rich field [14], many new aromatic ligands have also been found. In particular, the all-metal aromatic unit Al_4^{2-} was found in MAl_4^- (M=Li, Na, or Cu) complexes, and confirmed to be square planar with two delocalized π electrons [15]. It has also been demonstrated that the Al_4^{2-} unit can be complexed with transition metal or main-group metal atoms to form mononuclear sandwich-like complexes [16, 17]. In fact, some other all-metal aromatic species have also been investigated already [18]. Among them, the all-metal tetraatomic species of Group 5 elements E_4^{2-} (E=Sb, Bi) have been found in the isolated compounds $(2,2,2\text{-crypt-}K^+)_2Sb_4^{2-}$ and $(2,2,2\text{-crypt-}K^+)_2Bi_4^{2-}$, respectively [19, 20]. On the other hand, Sb_4^{2-} and Bi_4^{2-} are known as zintl anions, which can be used as building blocks for constructing solid materials [16, 17].

Similar to the Al_4^{2-} unit, these all-metal aromatic species E_4^{2-} (E=Sb, Bi), which are valence isoelectronic

to the classical aromatic $C_4H_4^{2-}$ dianion and possess six π electrons, have also been investigated in some half-sandwich and mononuclear sandwich-like complexes. Kuznetsov et al. [21] studied Sb_4^{2-} and $NaSb_4^-$ by ab initio calculations combined with photodetachment photoelectron spectroscopy and presented evidence that the global minimum structure of $NaSb_4^-$ was found to be square-pyramidal, i.e., consisting of a Na^+ ion coordinated to a Sb_4^{2-} square. Li et al. [22] studied a series of stable sandwich-like complexes $[Sb_4MSb_4]^{n-}$ (M=Fe, Ru, Os, Co, Rh, and Ir; n=1, or 2) at the B3LYP level of theory and found that the most stable structures of these complexes are the staggered D_{4d} conformers and the Sb_4^{2-} rings of them exhibit σ and π aromaticity. A series of mononuclear sandwich complexes $[Fe(\eta^4\text{-}E_4)_2]^{2-}$ (E=Sb, Bi) was also investigated by the same group via density functional theory (DFT) methods and it was confirmed that the aromaticity of these complexes can be attributed mostly to the effects of E–E π bonds and Fe lone pairs [23]. In addition, our previous work has proved using DFT that E_4^{2-} (E=Sb, Bi) can be complexed with boron atoms to form nonmetal-centered binuclear sandwich-like complexes $B_2(\eta^4\text{-}E_4)_2$ [24].

Since all-metal aromatic species E_4^{2-} (E=Sb, Bi) can act as ligands to form transition metal-centered mononuclear and nonmetal-centered binuclear sandwich-like complexes theoretically, can these E_4^{2-} species be used to sandwich the main-group metal atoms forming all-metal binuclear sandwich-like complexes? If so, are these all-metal binuclear sandwich-like complexes stable? Do they have some special properties? Thus, a series of all-metal binuclear sandwich-like complexes based on the all-metal aromatic units E_4^{2-} (E=Sb, Bi) and the main-group metal atoms M (M=Al, Ga, In), in which each metal atom has eight electrons in the valence shell (six electrons from the $\eta^4\text{-}E_4^{2-}$ ligand and two electrons from the shared electron pair of metal–metal single bond) and fulfills the octet rule, were designed. To the best of our knowledge, no such binuclear sandwich-like complexes have been reported to date. Therefore, in the present paper, a theoretical study was carried out on the equilibrium geometries and stabilities of the all-metal binuclear sandwich-like complexes of $M_2(\eta^4\text{-}E_4)_2$ (M=Al, Ga, In; E=Sb, Bi). The bonding nature and the aromaticity of these compounds were investigated by natural bond orbital (NBO) analysis and nucleus-independent chemical shifts (NICS).

Theoretical methods

Two DFT methods were used in this study. One functional is B3LYP, which incorporates Becke's three parameter functional (B3) [25] with the Lee, Yang, and Parr (LYP) [26] correlation functional. The other is BP86, which marries Becke's 1988 exchange functional (B) [27] with Perdew's [28] 1986 correlation functional. The 6-311+G(d) [29, 30] basis set was used for Al, Ga and the SDD [31, 32] basis set was used for In, Sb, Bi. The equilibrium geometries and vibrational frequencies of $M_2(\eta^4\text{-}E_4)_2$ (M=Al, Ga, In; E=Sb, Bi) were fully optimized by the B3LYP and BP86 methods. In order to provide insight into the bonding nature, the natural bond orbital (NBO) [33–36] analysis was also performed at the B3LYP/6-311+G(d)+SDD and B3LYP/SDD levels of theory for $M_2(\eta^4\text{-}E_4)_2$ (M=Al, Ga; E=Sb, Bi) and $In_2(\eta^4\text{-}E_4)_2$ (E=Sb, Bi), respectively. The nucleus independent chemical shifts (NICS) values of the most stable structures were also computed by the gauge including atomic orbital (GIAO) [37, 38] method at the same levels of theory to investigate the aromaticity of these complexes. All calculations were performed using the Gaussian 03 program package [39].

To further investigate the nature of the metal–metal interactions in $M_2(\eta^4\text{-}E_4)_2$ (M=Al, Ga, In; E=Sb, Bi), the bonding interactions between the two ME_4 fragments were analyzed with the energy decomposition scheme of the ADF 2010.02 program [40–42] at the BLYP/TZP level [25, 26] of theory. For heavy atoms indium, antimony and bismuth, scalar relativistic effects were considered using the zero-order regular approximation (ZORA) [43–48]. The binding energy ΔE_{bind} is divided into two major components:

$$\Delta E_{bind} = \Delta E_{prep} + \Delta E_{int} \quad (1)$$

The preparation energy ΔE_{prep} represents the amount of energy required to promote the fragments from their equilibrium geometries and electronic ground state to the structures and electronic state that they will have in the combined complex. The interaction energy, ΔE_{int}, between two fragments in a molecule can be divided into three main components:

$$\Delta E_{int} = \Delta E_{elstat} + \Delta E_{Pauli} + \Delta E_{orb} \quad (2)$$

In Eq. 2, ΔE_{elstat} gives the classical electrostatic interaction energy between the fragments, ΔE_{Pauli} corresponds to the repulsive interactions between the fragments, while ΔE_{orb} describes the orbital interactions between the occupied and virtual orbitals of the fragments. ΔE_{elstat} and ΔE_{orb}, can be considered as the estimate of the electrostatic and covalent contributions to the bonding, respectively. Therefore, the important information about the covalent and electrostatic character of the bond is given by the ratio $\Delta E_{orb}/(\Delta E_{orb}+\Delta E_{elstat})$ and $\Delta E_{elstat}/(\Delta E_{orb}+\Delta E_{elstat})$, respectively [49–51].

Results and discussion

The optimized geometrical structures for the $M_2(\eta^4\text{-}E_4)_2$ (M=Al, Ga, In; E=Sb, Bi) species are shown in Fig. 1, and

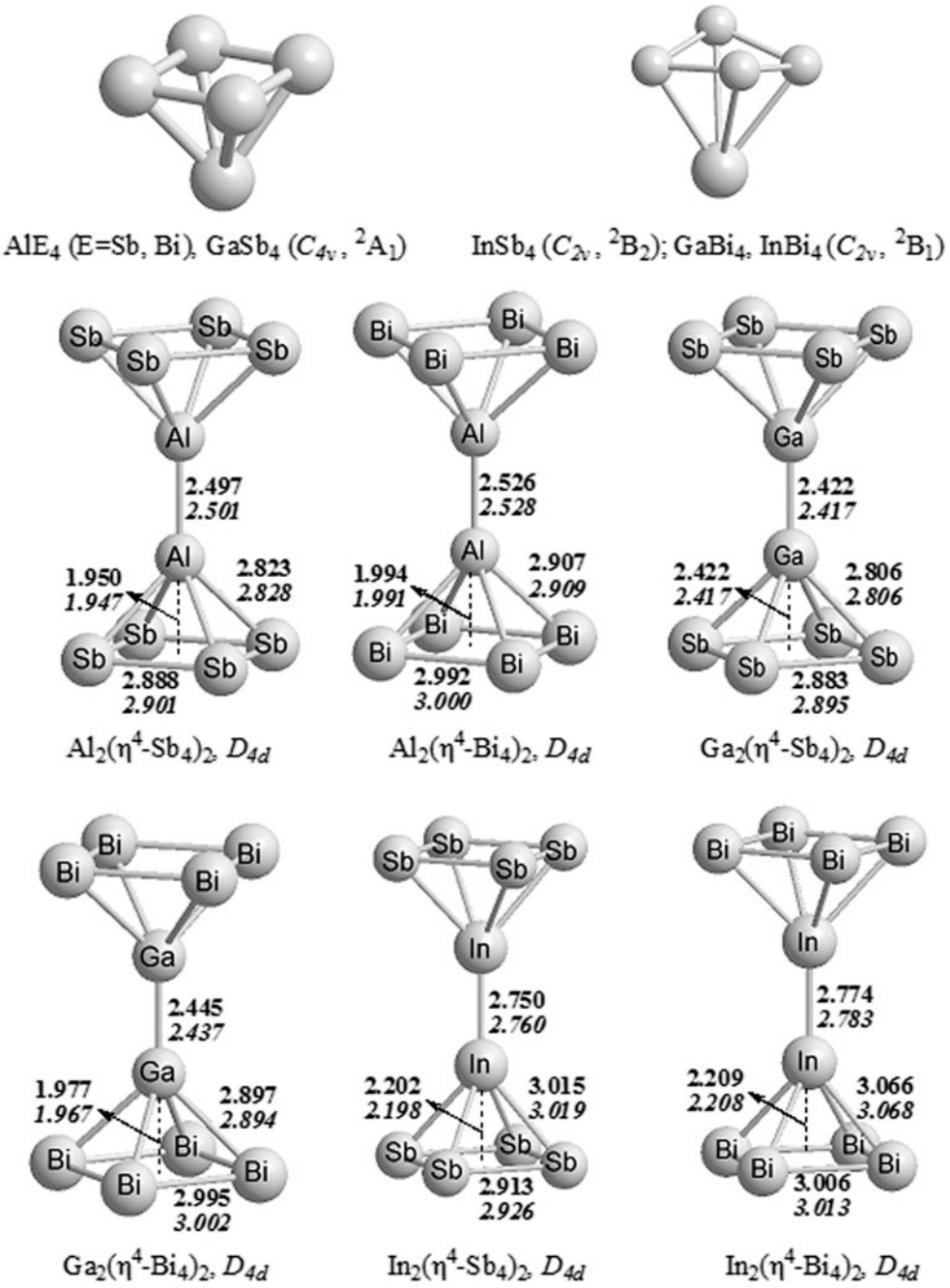

Fig. 1 Molecular structures for ME_4 and optimized geometries for the D_{4d} $M_2(\eta^4\text{-}E_4)_2$ (M=Al, Ga, In; E=Sb, Bi) species by the B3LYP (upper distances; *bold face*) and BP86 (lower distances; *italics*) methods. Distances are in Ångstroms

some relevant molecular orbitals for the centred metal–metal bonding of $Al_2(\eta^4\text{-}Sb_4)_2$ are given in Fig. 2. The two-step substitution reactions of CpZnZnCp to produce $M_2(\eta^4\text{-}E_4)_2$ are shown in Fig. 3 and some molecular orbitals for Sb_4^{2-} in the bare ring and the $Al_2(\eta^4\text{-}Sb_4)_2$ species are given in Fig. 4, respectively. Zero-point energies (ZPE), total energies after ZPE correction (E_{ZPE}), the number of imaginary frequencies (NIMAG), and the relative energies (RE) for $M_2(\eta^4\text{-}E_4)_2$ (M=Al, Ga, In; E=Sb, Bi) are summarized in Table 1, while the Wiberg bond indices (WBIs) of M–M, M–E, E–E and M, E atoms for each $M_2(\eta^4\text{-}E_4)_2$ species are listed in Table 3. The energy decomposition analysis (EDA) of $M_2(\eta^4\text{-}E_4)_2$ is tabulated in Table 4, while the dissociation energies of the $M_2(\eta^4\text{-}E_4)_2$ species are listed in Table 5, and the Gibbs free energy changes for the two reactions are shown in Tables 6 and 7. The calculated NICS values for $M_2(\eta^4\text{-}E_4)_2$ are given in Table 8.

Energies and geometrical structures of $M_2(\eta^4\text{-}E_4)_2$ (M=Al, Ga, In; E=Sb, Bi)

As shown in Table 1, the B3LYP and BP86 methods yield two conformers with D_{4d} and D_{4h} symmetry for each of the $M_2(\eta^4\text{-}E_4)_2$ (M=Al, Ga, In; E=Sb, Bi) species. As in the case

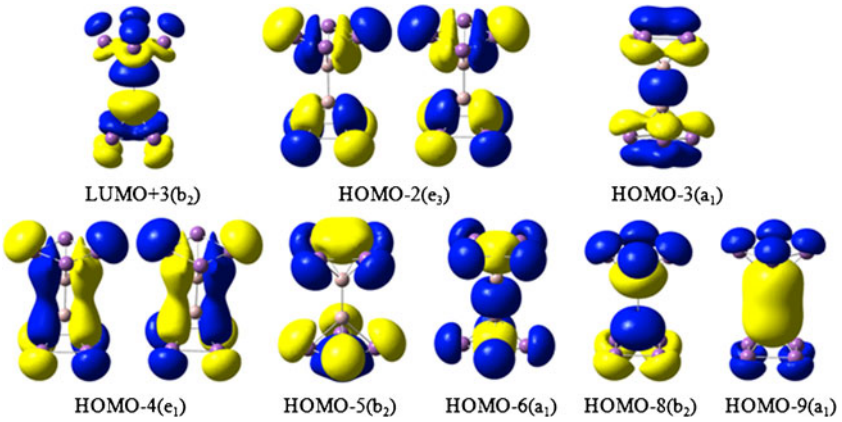

Fig. 2 Plot of some relevant molecular orbitals for the centred metal–metal bonding in $Al_2(\eta^4\text{-}Sb_4)_2$

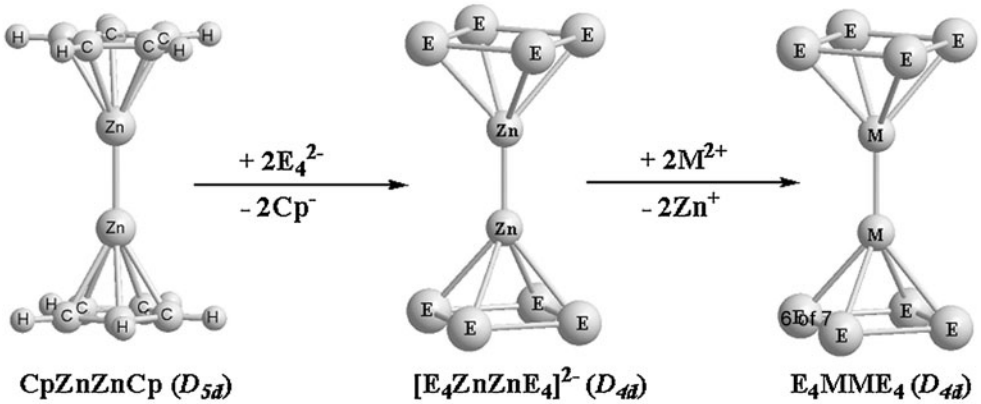

Fig. 3 The two-step substitution reactions of CpZnZnCp to produce $M_2(\eta^4\text{-}E_4)_2$ (M=Al, Ga, In; E=Sb, Bi)

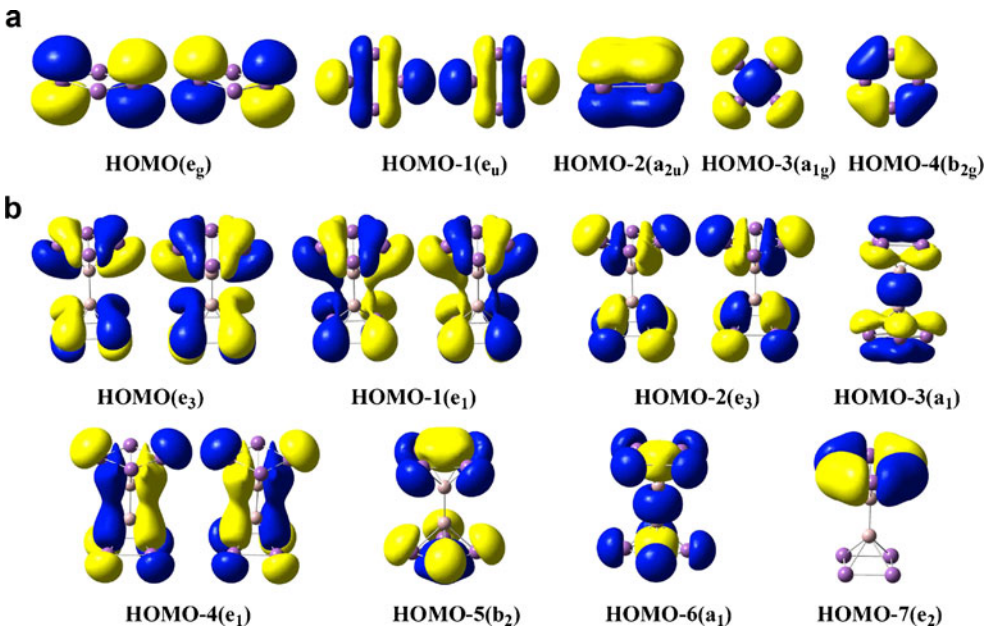

Fig. 4 Some molecular orbital pictures for Sb_4^{2-} in the bare ring (**a**) and the $Al_2(\eta^4\text{-}Sb_4)_2$ species (**b**)

Table 1 Total energies (E_{ZPE}, in Hartrees), zero-point energies (ZPE, in kcal mol^{-1}), the number of imaginary vibrational frequencies (NIMAG) and the relative energies (RE, in kcal mol^{-1}) for $M_2(\eta^4\text{-}E_4)_2$ (M=Al, Ga, In; E=Sb, Bi)

Species		B3LYP				BP86			
		E_{ZPE}	ZPE	NIMAG	RE	E_{ZPE}	ZPE	NIMAG	RE
$Al_2(\eta^4\text{-}Sb_4)_2$	D_{4d}	−528.615806	4.76	1[a]	0.00	−528.950351	4.73	1[a]	0.00
$Al_2(\eta^4\text{-}Sb_4)_2$	D_{4h}	−528.615633	4.76	0	0.11	−528.950189	4.74	0	0.10
$Al_2(\eta^4\text{-}Bi_4)_2$	D_{4d}	−528.469514	3.95	0	0.00	−528.785331	3.94	0	0.00
$Al_2(\eta^4\text{-}Bi_4)_2$	D_{4h}	−528.469365	3.95	1	0.09	−528.785200	3.94	1	0.08
$Ga_2(\eta^4\text{-}Sb_4)_2$	D_{4d}	−3893.466322	4.05	1[a]	0.00	−3,894.227823	4.02	1[a]	0.00
$Ga_2(\eta^4\text{-}Sb_4)_2$	D_{4h}	−3893.466133	4.07	0	0.12	−3,894.227650	4.04	0	0.11
$Ga_2(\eta^4\text{-}Bi_4)_2$	D_{4d}	−3893.316134	3.24	1[a]	0.00	−3,894.059495	3.24	0	0.00
$Ga_2(\eta^4\text{-}Bi_4)_2$	D_{4h}	−3893.315985	3.24	1	0.09	−3,894.059364	3.25	1	0.08
$In_2(\eta^4\text{-}Sb_4)_2$	D_{4d}	−47.482038	3.54	1[a]	0.00	−47.851404	3.52	1[a]	0.00
$In_2(\eta^4\text{-}Sb_4)_2$	D_{4h}	−47.481978	3.55	0	0.04	−47.851350	3.54	0	0.03
$In_2(\eta^4\text{-}Bi_4)_2$	D_{4d}	−47.357917	2.92	1[a]	0.00	−47.706342	2.90	1[a]	0.00
$In_2(\eta^4\text{-}Bi_4)_2$	D_{4h}	−47.357866	2.92	0	0.03	−47.706302	2.91	0	0.03

[a] When the finer grid (Grid=120, 974) is used, the imaginary vibrational frequencies disappear

of the $M_2(\eta^4\text{-}E_4)_2$ species with one imaginary vibrational frequency, all real vibrational frequencies were found when the finer grid (Grid=120, 974) was used, except for the D_{4h} $M_2(\eta^4\text{-}Bi_4)_2$ (M=Al, Ga) conformers with a very small imaginary vibrational frequency (less than $2i$ cm^{-1}). The energy differences between the D_{4d} and D_{4h} conformers of $M_2(\eta^4\text{-}E_4)_2$ are predicted to be negligible (<0.12 kcal mol^{-1}). In addition, the distances for the two all-metal $\eta^4\text{-}E_4^{2-}$ ligands are greater than 6.4 Å, indicating that the two ligands exhibit essentially free rotation. Therefore, experiments may observe $M_2(\eta^4\text{-}E_4)_2$ with $D_{\infty h}$ symmetry. Hence, only the D_{4d} $M_2(\eta^4\text{-}E_4)_2$ structures are shown in Fig. 1. As shown in Fig. 1 and Table 1, the results calculated for $M_2(\eta^4\text{-}E_4)_2$ (M=Al, Ga, In; E=Sb, Bi) by the B3LYP and BP86 methods are almost identical. Furthermore, theoretical results of some metallocenes by the B3LYP method are in reasonable agreement with those of available experiments [52]. In general, only the B3LYP results are used for the following discussion.

As shown in Fig. 1, for the $M_2(\eta^4\text{-}E_4)_2$ species, the Al–Al, Ga–Ga and In–In bond distances are all shorter than the experimental Al–Al (2.660 Å) [53], Ga–Ga (2.541 Å) [54] and In–In (2.828 Å) [55] single bond lengths in $R_2M\text{-}MR_2$ [M=Al, Ga, In; R=CH(SiMe$_3$)$_2$], respectively. At the same time, the Al–Al and Ga–Ga bond lengths in $R_2M\text{-}MR_2$ [M=Al, Ga] were also calculated at the B3LYP/6-311+G (d, p) level of theory, while the In–In bond length in $R_2In\text{-}InR_2$ was calculated at the B3LYP/6-311+G (d,p)+SDD level of theory (Table 2). As listed in Table 2, the caculated M–M bond lengths in $R_2M\text{-}MR_2$ are all slightly longer than those of the experimental bond lengths, indicating that there is significant bonding between the two centred metal atoms in each of the $M_2(\eta^4\text{-}E_4)_2$ species and that the all-metal $\eta^4\text{-}E_4^{2-}$ ligands can stabilize the centred metal–metal bonds to form all-metal binuclear sandwich-like complexes. In addition, with the same centred metal, the M–M bond distance of $M_2(\eta^4\text{-}Sb_4)_2$ is shorter than that of the corresponding $M_2(\eta^4\text{-}Bi_4)_2$, suggesting that $\eta^4\text{-}Sb_4^{2-}$ ligands have a greater ability to stabilize metal–metal bonds than $\eta^4\text{-}Bi_4^{2-}$ ligands. This result is in accordance with that of the nonmetal-centered binuclear sandwich-like complexes $B_2(\eta^4\text{-}Sb_4)_2$ and $B_2(\eta^4\text{-}Bi_4)_2$ [24]. While for the M–E bond distances, with the same centred metal, lighter atoms for E have shorter M–E distances. The Sb–Sb and Bi–Bi bond distances of the all-metal ligands are about 2.9 and 3.0 Å, respectively, which are close to the corresponding experimental Sb–Sb and Bi–Bi bond lengths (2.75 and 2.94 Å) in (2,2,2-crypt-K$^+$)$_2$Sb$_4^{2-}$ and (2,2,2-crypt-K$^+$)$_2$Bi$_4^{2-}$ compounds [19, 20].

NBO analysis of $M_2(\eta^4\text{-}E_4)_2$ (M=Al, Ga, In; E=Sb, Bi)

As listed in Table 3, according to NBO analysis, the wiberg bond indices (WBIs) of M–M bonds in the $M_2(\eta^4\text{-}E_4)_2$ species are between 0.896 and 0.962, which are close to

Table 2 The M–M bond lengths by the B3LYP method for $M_2(\eta^4\text{-}E_4)_2$ (M=Al, Ga, In; E=Sb, Bi), $R_2M\text{-}MR_2$ [M=Al, Ga, In; R=CH(SiMe$_3$)$_2$], and the experimental M–M bond lengths for $R_2M\text{-}MR_2$

Bond length	$M_2(\eta^4\text{-}Sb_4)_2$	$M_2(\eta^4\text{-}Bi_4)_2$	$R_2M\text{-}MR_2$	Exp. $R_2M\text{-}MR_2$
Al–Al	2.497	2.526	2.663	2.660 [53]
Ga–Ga	2.422	2.445	2.607	2.541 [54]
In–In	2.750	2.774	2.901	2.828 [55]

Table 3 Wiberg bond indices (WBIs) of M–M, M–E, E–E and M, E atoms by the B3LYP method for the $M_2(\eta^4\text{-}E_4)_2$ (M=Al, Ga, In; E=Sb, Bi) species

Species	M-M	M-E	E-E	M	E
$Al_2(\eta^4\text{-}Sb_4)_2$ (D_{4d})	0.962	0.687	1.039	3.777	3.001
$Al_2(\eta^4\text{-}Bi_4)_2$ (D_{4d})	0.950	0.696	1.042	3.807	2.994
$Ga_2(\eta^4\text{-}Sb_4)_2$ (D_{4d})	0.959	0.679	1.037	3.754	2.996
$Ga_2(\eta^4\text{-}Bi_4)_2$ (D_{4d})	0.936	0.677	1.040	3.738	2.993
$In_2(\eta^4\text{-}Sb_4)_2$ (D_{4d})	0.897	0.580	1.078	3.312	3.011
$In_2(\eta^4\text{-}Bi_4)_2$ (D_{4d})	0.896	0.600	1.080	3.396	3.013

the standard value of single bond (1.0), indicating that a single M–M bond exists in each of these species.

The WBIs of M–E bonds in the $M_2(\eta^4\text{-}E_4)_2$ species are in the range of 0.580–0.696, suggesting that the M–E bonding in each of these species is covalent. This is consistent with the covalent boron-ligand bonds in $B_2(\eta^4\text{-}E_4)_2$ (E=Sb, Bi) [24] but different from the ionic metal-ligand bonds in the first stable binuclear metallocene Cp*ZnZnCp* (Cp*=C_5Me_5) [9]. The WBIs of E–E bonds in the all-metal $\eta^4\text{-}E_4^{2-}$ ligands are between 1.037 and 1.080, indicating the existence of electronic delocalization in these all-metal ligands. In addition, the total WBIs for the centred metal atoms are from 3.312 to 3.807, and the WBIs for the atoms of the all-metal ligands are close to 3.00.

Energy decomposition analysis

As shown in Table 4, for all the $M_2(\eta^4\text{-}E_4)_2$ species, the interaction energies ΔE_{int} to the metal–metal bonds are from −60.68 to −38.86 kcal mol^{-1}, and the binding energies ΔE_{bind} are between −60.30 to −13.58 kcal mol^{-1}. For the same ligand, the absolute value of ΔE_{int} and ΔE_{bind} are in the order of $Al_2(\eta^4\text{-}E_4)_2 > Ga_2(\eta^4\text{-}E_4)_2 > In_2(\eta^4\text{-}E_4)_2$, which indicates that, with increasing metallicity of the centred metal, the metal–metal bonds become weaker gradually, while with the same centred metal, the ΔE_{int} and ΔE_{bind} values of $M_2(\eta^4\text{-}Sb_4)_2$ are more negative than those of the corresponding $M_2(\eta^4\text{-}Bi_4)_2$, suggesting that $M_2(\eta^4\text{-}Sb_4)_2$ is more stable than the corresponding $M_2(\eta^4\text{-}Bi_4)_2$ and lighter ligands have greater ability to stabilize metal–metal bonds. This is consistent with the prediction that the metal–metal bond lengths of $M_2(\eta^4\text{-}Sb_4)_2$ are shorter than those of $M_2(\eta^4\text{-}Bi_4)_2$, whereas, due to the large positive preparation energy ΔE_{prep} of the $GaBi_4$ and InE_4 (E=Sb, Bi) mononuclear fragments, the absolute values of ΔE_{bind} for $Ga_2(\eta^4\text{-}Bi_4)_2$ and $In_2(\eta^4\text{-}E_4)_2$ (E=Sb, Bi) are much smaller than those of other species.

Furthermore, for all the $M_2(\eta^4\text{-}E_4)_2$ species, the orbital interaction energy ΔE_{orb} values are more negative than the corresponding electrostatic interaction energy ΔE_{elstat} values, indicating that the covalent contributions ΔE_{orb} are larger than the electrostatic contributions ΔE_{elstat}. Therefore, the metal–metal bonds in $M_2(\eta^4\text{-}E_4)_2$ have a greater degree of covalent character, which is consistent with the WBIs of the metal–metal bonds. In addition, it can be seen from Table 4 that only the a_1 and e orbitals contribute to the ΔE_{orb} term and the orbital interactions come mainly from the a_1 orbitals, which give 95–97% of total orbital interaction energy ΔE_{orb}, while the e orbitals make very little contribution to the ΔE_{orb} term.

Molecular orbital analysis

To further investigate the nature of the centred metal–metal bonding in these all-metal binuclear sandwich-like complexes $M_2(\eta^4\text{-}E_4)_2$ (M=Al, Ga, In; E=Sb, Bi), envelope plots

Table 4 Energy decomposition analysis (EDA) of metal–metal bonds (using the fragments ME_4 + ME_4) of the D_{4d} $M_2(\eta^4\text{-}E_4)_2$(M=Al, Ga, In; E=Sb, Bi) species at the BLYP/TZP level of theory (energy values are in kcal mol^{-1})

Species	$Al_2(\eta^4\text{-}Sb_4)_2$	$Al_2(\eta^4\text{-}Bi_4)_2$	$Ga_2(\eta^4\text{-}Sb_4)_2$	$Ga_2(\eta^4\text{-}Bi_4)_2$	$In_2(\eta^4\text{-}Sb_4)_2$	$In_2(\eta^4\text{-}Bi_4)_2$
ΔE_{bind}	−60.30	−55.23	−48.69	−21.27	−15.02	−13.58
ΔE_{int}	−60.68	−55.67	−49.61	−44.22	−43.10	−38.86
ΔE_{Pauli}	142.08	137.84	138.23	132.86	117.72	112.43
ΔE_{elstat}[a]	−49.90	−50.98	−56.21	−57.10	−51.35	−51.60
	24.6%	26.3%	29.9%	32.2%	31.9%	34.1%
ΔE_{orb}[a]	−152.86	−142.53	−131.63	−119.98	−109.47	−99.69
	75.4%	73.7%	70.1%	67.8%	68.1%	65.9%
A_1[b]	−148.39	−137.62	−125.94	−114.23	−105.75	−96.07
	97.1%	96.6%	95.7%	95.2%	96.6%	96.4%
A_2	0.00	0.00	0.00	0.00	0.00	0.00
B_1	−0.03	−0.03	−0.02	−0.01	0.00	0.00
B_2	−0.03	−0.03	−0.02	−0.02	0.00	0.00
E_1	−4.42	−4.86	−5.66	−5.72	−3.70	−3.62
	2.9%	3.4%	4.3%	4.8%	3.4%	3.6%
ΔE_{prep}	0.38	0.44	0.92	22.95	28.08	25.28

[a]Values in parentheses give the percentage contribution to metal–metal bonding

[b]Values in parentheses give the percentage contribution to total orbital interactions

of some relevant MOs of the model compound $Al_2(\eta^4\text{-}Sb_4)_2$ are shown in Fig. 2.

As shown by EDA analysis, the a_1 and e orbitals are the main contributors to the covalent bonds between the two ME_4 fragments, which can also be presented by MOs. As shown by the MO plots (Fig. 2), the degenerate occupied molecular orbitals HOMO-4(e_1) give a pictorial description of the Al-Al π-bonding, while the degenerate HOMO-2(e_3) are the corresponding Al–Al π-antibonding orbitals. They originated mainly from the interaction of p_x-p_x or p_y-p_y orbitals of the two aluminum atoms, respectively, with participation of the antimony p_z orbitals of the ligands $\eta^4\text{-}Sb_4^{2-}$. HOMO-3(a_1), HOMO-6(a_1) and HOMO-9(a_1) show mainly Al–Al σ-bonding orbitals, which result from the interactions of s and p_z orbitals of the two aluminum atoms. This contrasts with the Zn-Zn σ bond in Cp*ZnZnCp* (Cp*=C_5Me_5), which involves mostly the Zn 4s orbital [9, 56], while HOMO-9 (a_1) also makes a small contribution to the Al–Sb_4^{2-} interaction. In addition, HOMO-5(b_2), HOMO-8(b_2) and the unoccupied molecular orbital LUMO+3(b_2) are the corresponding Al–Al σ-antibonding orbitals of HOMO-6(a_1), HOMO-9(a_1) and HOMO-3(a_1), respectively.

Stabilities of the complexes

The stability of the all-metal binuclear sandwich-like complexes $M_2(\eta^4\text{-}E_4)_2$ (M=Al, Ga, In; E=Sb, Bi) was estimated through the reactions of $M_2(\eta^4\text{-}E_4)_2 \rightarrow 2\ M(\eta^4\text{-}E_4)$ and $M_2(\eta^4\text{-}E_4)_2 \rightarrow 2\ M+2E_4$ by the B3LYP method. The dissociation energies, namely, ΔE_1 for $M_2(\eta^4\text{-}E_4)_2 \rightarrow 2\ M(\eta^4\text{-}E_4)$, which refers to breaking of the metal–metal bond, and ΔE_2 for $M_2(\eta^4\text{-}E_4)_2 \rightarrow 2\ M+2E_4$, including zero-point vibrational energy (ZPVE) corrections are listed in Table 5.

The most stable structures of the fragments ME_4 (M=Al, Ga, In; E=Sb, Bi) were also optimized (Fig. 1). As shown in Fig. 1, fragments AlE_4 (E=Sb, Bi) and $GaSb_4$ have C_{4v} symmetry, while fragments $GaBi_4$ and InE_4 (E=Sb, Bi) are of C_{2v} symmetry.

As listed in Table 5, for all the $M_2(\eta^4\text{-}E_4)_2$ species, the dissociation energies ΔE_1 are from 21.6 to 59.3 kcal mol^{-1}, whereas the dissociation energies ΔE_2 are between 59.6 and 127.7 kcal mol^{-1}, which are much higher than those of the corresponding ΔE_1. This suggests that the dissociation reaction of $M_2(\eta^4\text{-}E_4)_2 \rightarrow 2\ M(\eta^4\text{-}E_4)$ is easier to undergo than the reaction of $M_2(\eta^4\text{-}E_4)_2 \rightarrow 2\ M+2E_4$. Moreover, with the same ligand, the dissociation energies ΔE_1 and ΔE_2 of $Al_2(\eta^4\text{-}E_4)_2$ are highest, while those for $In_2(\eta^4\text{-}E_4)_2$ are lowest, indicating that the stability of these species is in the order of $Al_2(\eta^4\text{-}E_4)_2 > Ga_2(\eta^4\text{-}E_4)_2 > In_2(\eta^4\text{-}E_4)_2$ according to the two reactions. With the same centred metal, the dissociation energies ΔE_1 and ΔE_2 of $M_2(\eta^4\text{-}Sb_4)_2$ are higher than those of the corresponding $M_2(\eta^4\text{-}Bi_4)_2$, which suggests that $\eta^4\text{-}Sb_4^{2-}$ in the all-metal complexes $M_2(\eta^4\text{-}E_4)_2$ has a stronger ability to stabilize metal–metal bonds than $\eta^4\text{-}Bi_4^{2-}$, which is similar to the $\eta^4\text{-}E_4^{2-}$ ligands in $B_2(\eta^4\text{-}E_4)_2$ (E=Sb, Bi) [24].

Furthermore, as shown in Table 5, for $Al_2(\eta^4\text{-}Sb_4)_2$, $Al_2(\eta^4\text{-}Bi_4)_2$ and $Ga_2(\eta^4\text{-}Sb_4)_2$, the metal–metal bond dissociation energies ΔE_1 are 59.3, 52.2 and 54.1 kcal mol^{-1}, respectively, which are close to the Zn–Zn bond dissociation energies of the first stable binuclear metallocene Cp*ZnZnCp* (Cp*=C_5Me_5) at the B3LYP/6-31G(d)+SDD and CCSD(T)//B3LYP/6-31G(d)+SDD levels of theory [9], indicating the existence of substantial metal–metal bonds in these species. Thus, with respect to the dissociation reaction, $M_2(\eta^4\text{-}E_4)_2 \rightarrow 2\ M(\eta^4\text{-}E_4)$, the $Al_2(\eta^4\text{-}Sb_4)_2$, $Al_2(\eta^4\text{-}Bi_4)_2$ and $Ga_2(\eta^4\text{-}Sb_4)_2$ species appear to be very stable. However, for $Ga_2(\eta^4\text{-}Bi_4)_2$, the Ga–Ga bond dissociation energy is only 25.8 kcal mol^{-1}, which is close to the In–In bond dissociation energies for $In_2(\eta^4\text{-}E_4)_2$ (E=Sb, Bi), indicating the relatively weak metal–metal bonds in these species. These relatively low dissociation energies of $Ga_2(\eta^4\text{-}Bi_4)_2$ and $In_2(\eta^4\text{-}E_4)_2$ (E=Sb, Bi) may be due to the large structural differences between the ME_4 structures in $M_2(\eta^4\text{-}E_4)_2$ and their equilibrium geometries, which are from C_{4v} to C_{2v} symmetry. All these results are in accordance with the predictions of EDA analysis.

Table 5 Dissociation energies (kcal mol^{-1}) for $M_2(\eta^4\text{-}E_4)_2 \rightarrow 2\ M(\eta^4\text{-}E_4)$ (ΔE_1) and $M_2(\eta^4\text{-}E_4)_2 \rightarrow 2\ M+2E_4$ (ΔE_2) by the B3LYP method (including ZPVE corrections)

Species	ΔE_1	ΔE_2
$Al_2(\eta^4\text{-}Sb_4)_2$ (D_{4d})	59.3	127.7
$Al_2(\eta^4\text{-}Bi_4)_2$ (D_{4d})	52.2	95.7
$Ga_2(\eta^4\text{-}Sb_4)_2$ (D_{4d})	54.1	111.7
$Ga_2(\eta^4\text{-}Bi_4)_2$ (D_{4d})	25.8	77.2
$In_2(\eta^4\text{-}Sb_4)_2$ (D_{4d})	22.6	77.7
$In_2(\eta^4\text{-}Bi_4)_2$ (D_{4d})	21.6	59.6

A possible synthetic route to $M_2(\eta^4\text{-}E_4)_2$ (M=Al, Ga, In; E=Sb, Bi)

In order to explore a possible synthetic route to these stable all-metal binuclear sandwich-like complexes $M_2(\eta^4\text{-}E_4)_2$ (M=Al, Ga, In; E=Sb, Bi), two-step substitution reactions, namely, $CpZnZnCp+2E_4^{2-} \rightarrow [E_4ZnZnE_4]^{2-}+2Cp^-$ and $[E_4ZnZnE_4]^{2-}+2\ M^{2+} \rightarrow E_4MME_4+2Zn^+$ were also investigated by the B3LYP method (Fig. 3). The Gibbs free energy changes, ΔG, of these reactions are given in Tables 6 and 7.

Table 6 Gibbs free energy changes (ΔG, kcal mol^{-1}) for $CpZnZnCp+2E_4^{2-} \rightarrow [E_4ZnZnE_4]^{2-}+2Cp^-$ by the B3LYP method

Reactions	ΔG
$CpZnZnCp + 2Sb_4^{2-} \rightarrow [Sb_4ZnZnSb_4]^{2-} + 2Cp^-$	−136.5
$CpZnZnCp + 2Bi_4^{2-} \rightarrow [Bi_4ZnZnBi_4]^{2-} + 2Cp^-$	−136.6

Table 7 Gibbs free energy changes (ΔG, kcal mol^{-1}) for $[E_4ZnZnE_4]^{2-}$+2 M^{2+}→E_4MME_4 +2Zn^+ by the B3LYP method

Reactions	ΔG		
	M(Al)	M(Ga)	M(In)
$[Sb_4ZnZnSb_4]^{2-}$ + 2 M^{2+}→ Sb_4MMSb_4 + 2Zn^+	−758.0	−817.1	−668.3
$[Bi_4ZnZnBi_4]^{2-}$ + 2 M^{2+}→ Bi_4MMBi_4 + 2Zn^+	−777.5	−830.8	−697.8

As shown in Table 6, the reactions of the Cp ligands substituted by the all-metal η^4-E_4^{2-} ligands are predicted to be −136.5 and −136.6 kcal mol^{-1}, respectively, suggesting that the relative stability of these $[Sb_4ZnZnSb_4]^{2-}$ and $[Bi_4ZnZnBi_4]^{2-}$ species. As tabulated in Table 7, the Gibbs free energy changes for the reactions of Zn atoms substituted by Al, Ga and In atoms are from −668.3 to −830.8 kcal mol^{-1}. These high negative values indicate that these all-metal binuclear sandwich-like complexes are very stable. It should be noted that although $Ga_2(\eta^4\text{-}Bi_4)_2$ and $In_2(\eta^4\text{-}E_4)_2$ (E=Sb, Bi) have relatively low dissociation energies according to the reaction of $M_2(\eta^4\text{-}E_4)_2$→2 $M(\eta^4\text{-}E_4)$, the Gibbs free energy changes for the reactions of Zn atoms substituted by In atoms are −830.8, −668.3 and −697.8 kcal mol^{-1}, respectively. Therefore, these $M_2(\eta^4\text{-}E_4)_2$ species can be synthesized through these two-step substitution reactions.

Aromaticity of E_4^{2-} for the $M_2(\eta^4\text{-}E_4)_2$ (M=Al, Ga, In; E=Sb, Bi) species

The concept of aromaticity was introduced by August Kekulé in 1865 [57]. The terms "aromatic" and "aromaticity" are used to describe cyclic, planar, and conjugated molecule structures with (4n+2) pi-electrons. There are many criteria of aromaticity, such as structural, energetic, and magnetic criteria [57–62]. Among them, the NICS criterion, which is based on the absolute magnetic shieldings computed at or above ring centers, is used widely and has proved a simple and efficient aromaticity probe [63]. Negative and positive NICS values denote aromaticity and antiaromaticity, respectively, while NICS values close to zero indicate nonaromaticity. More negative NICS value signals more aromatic character of the system [63, 64]. NICS(0.0) and NICS(1.0), which is calculated at the center and above the center by 1.0 Å of the square describe the σ aromaticity and π aromaticity of the system, respectively [65, 66]. In organic and inorganic compounds, multiple aromaticity (σ and π), multiple antiaromaticity (σ and π), and conflicting aromaticity (simultaneous presence of σ aromaticity and π antiaromaticity or σ antiaromaticity and π aromaticity) are very rare, but in all-metal aromatic systems they seems to be much more common [18].

As shown in Table 8, for the all-metal Al_4^{2-} unit, which has been reported to exhibit characteristics of multiple aromaticity [15], the NICS(0.0) and NICS(1.0) values are all negative. This also indicates that Al_4^{2-} has multiple aromaticity (σ and π). Different from Al_4^{2-}, in the nonmetal-centered binuclear sandwich-like complexes $B_2(\eta^4\text{-}Bi_4)_2$, the η^4-Bi_4^{2-} ligands possess antiaromaticity [24]. However, for the all-metal η^4-E_4^{2-} ligands in the $M_2(\eta^4\text{-}E_4)_2$ (M=Al, Ga, In; E=Sb, Bi) species, the NICS(0.0) values are all positive, whereas NICS(1.0) values are all negative suggesting σ antiaromaticity and π aromaticity of the all-metal η^4-E_4^{2-} ligands after complexation with these main-group metal atoms. Therefore, these all-metal η^4-E_4^{2-} (E=Sb, Bi) ligands should be considered to have conflicting aromaticity (σ antiaromaticity and π aromaticity).

Furthermore, as listed in Table 8, for all the $M_2(\eta^4\text{-}E_4)_2$ speices, η^4-Sb_4^{2-} ligands have more negative NICS(1.0) values than η^4-Bi_4^{2-} ligands. In addition, with the same ligands, the $Ga_2(\eta^4\text{-}E_4)_2$ species have the most negative NICS(1.0) values, while the $In_2(\eta^4\text{-}E_4)_2$ species have the most positive NICS(0.0) values. Thus, in these $M_2(\eta^4\text{-}E_4)_2$ speices, with the same ring, the π aromaticity of $Ga_2(\eta^4\text{-}E_4)_2$ is the largest and $In_2(\eta^4\text{-}E_4)_2$ possesses the largest σ antiaromaticity.

In order to provide further evidence of aromaticity for η^4-E_4^{2-} in $M_2(\eta^4\text{-}E_4)_2$, some MOs of the model systems Sb_4^{2-} and $Al_2(\eta^4\text{-}Sb_4)_2$ were also analyzed (Fig. 4).

As presented in Fig. 4a, for the Sb_4^{2-} dianion, the degenerate highest occupied molecular orbitals HOMO(e_g) and the occupied molecular orbitals HOMO-2(a_{2u}) are π orbitals, which come from p_z atomic orbitals (AOs) of the antimony atoms. Thus, Sb_4^{2-} possesses six π electrons and can be considered to be π-aromatic, while the HOMO-1(e_u),

Table 8 Nucleus-independent chemical shifts (NICS) values (in ppm) for Al_4^{2-}, and the $M_2(\eta^4\text{-}E_4)_2$ (M=Al, Ga, In; E=Sb, Bi) species calculated by the B3LYP method

Species	Al_4^{2-} (D_{4h})	$Al_2(\eta^4\text{-}Sb_4)_2$ (D_{4d})	$Al_2(\eta^4\text{-}Bi_4)_2$ (D_{4d})	$Ga_2(\eta^4\text{-}Sb_4)_2$ (D_{4d})	$Ga_2(\eta^4\text{-}Bi_4)_2$ (D_{4d})	$In_2(\eta^4\text{-}Sb_4)_2$ (D_{4d})	$In_2(\eta^4\text{-}Bi_4)_2$ (D_{4d})
NICS (0.0)	−34.45	5.70	6.58	5.31	7.39	8.63	9.14
NICS (1.0)	−27.39	−9.38	−7.20	−17.20	−14.82	−6.79	−5.45

HOMO-3(a_{1g}) and HOMO-4(b_{2g}) are delocalized σ orbitals. Moreover, the HOMO-3(a_{1g}) oriented radially towards the center of the square from the $p_{x,y}$ AOs of the antimony atoms, and belongs to the radially oriented molecular orbital (r-MO), while the HOMO-4(b_{2g}) is considered a tangentially oriented molecular orbital (t-MO), which is oriented tangentially around the square from the $p_{x,y}$ AOs of the antimony atoms. Therefore, the HOMO-3(a_{1g}) and the HOMO-4(b_{2g}) are the r-MO and t-MO for Sb_4^{2-}, respectively, which are similar to the two delocalized σ MOs of Al_4^{2-} [15]. However, unlike Al_4^{2-}, except for the two electron pairs occupied the r-MO and t-MO of Sb_4^{2-}, two additional electron pairs have entered the degenerate HOMO-1(e_u), which are also considered to be t-MOs, and result in σ-antiaromatic character of Sb_4^{2-}.

When the Sb_4^{2-} dianions are complexed with aluminum atoms to form $Al_2(\eta^4\text{-}Sb_4)_2$, there are five π orbitals for $\eta^4\text{-}Sb_4^{2-}$, the degenerate HOMO-2(e_3), the HOMO-3(a_1) and the degenerate HOMO-4(e_1) (Fig. 4b), which confirm the presence of π aromaticity for $\eta^4\text{-}Sb_4^{2-}$ in $Al_2(\eta^4\text{-}Sb_4)_2$. In addition, seven delocalized σ orbitals are found for $\eta^4\text{-}Sb_4^{2-}$ in $Al_2(\eta^4\text{-}Sb_4)_2$, namely, the degenerate HOMO(e_3), the degenerate HOMO-1(e_1), the HOMO-5(b_2), the HOMO-6 (a_1) and the HOMO-7(e_2). Among them, the HOMO-5(b_2) and the HOMO-6(a_1) are two r-MOs, while the degenerate HOMO(e_3), the degenerate HOMO-1(e_1) and the HOMO-7 (e_2) are the t-MOs, which indicate σ antiaromaticity of the $\eta^4\text{-}Sb_4^{2-}$ ligands in $Al_2(\eta^4\text{-}Sb_4)_2$. Therefore, the all-metal $\eta^4\text{-}E_4^{2-}$ dianion in $M_2(\eta^4\text{-}E_4)_2$ should be considered as π-aromatic and σ-antiaromatic, which is consistent with the results of the NICS index.

Summary and conclusions

Theoretical studies found that the all-metal aromatic units E_4^{2-} (E=Sb, Bi) can act as ligands to form all-metal binuclear sandwich-like complexes $M_2(\eta^4\text{-}E_4)_2$ (M=Al, Ga, In; E=Sb, Bi). For these all-metal complexes, the staggered D_{4d} conformers are predicted to be stable. The centred metal–metal bonds are all covalent single bonds that are derived mostly from the s and p_z orbitals of the centred metal atoms, while the a_1 and e orbitals are the main contributors to these centred metal–metal covalent bonds. The metal–ligand interactions in these species are all covalent, and lighter ligands have stronger ability to stabilize the metal–metal bonds. NICS values and MO analysis suggest that the all-metal $\eta^4\text{-}E_4^{2-}$ ligands in $M_2(\eta^4\text{-}E_4)_2$ possess conflicting aromaticity (σ antiaromaticity and π aromaticity), which differs from the multiple aromatic unit Al_4^{2-} and the antiaromatic ligands $\eta^4\text{-}Bi_4^{2-}$ in $B_2(\eta^4\text{-}Bi_4)_2$. The dissociation energies of the centred metal–metal bonds of the $Al_2(\eta^4\text{-}Sb_4)_2$, $Al_2(\eta^4\text{-}Bi_4)_2$ and $Ga_2(\eta^4\text{-}Sb_4)_2$ species are close to that of the Zn–Zn bond in the first stable binuclear metallocene Cp*ZnZnCp* indicating the existence of significant bonding between the two centred metal atoms in these species. These stable complexes can be prepared through two step substitution reactions, namely, $CpZnZnCp + 2E_4^{2-} \rightarrow [E_4ZnZnE_4]^{2-} + 2Cp^-$ and $[E_4ZnZnE_4]^{2-} + 2\ M^{2+} \rightarrow E_4MME_4 + 2Zn^+$.

Acknowledgments We are indebted to the Chinese National Natural Science Foundation (20903010), Research Fund for the Doctoral Program of Higher Education (200800071019), and Project of State Key Laboratory of Explosion Science of Technology (Beijing Institute of Technology) (2DkT10-01a).

References

1. Kealy TJ, Pauson PL (1961) Nature 168:1039–1040
2. Rogers RD, Atwood JL, Foust D, Rauch MD (1981) J Cryst And Mol Struc 11:183–188
3. Flower KR, Hitchcock PB (1996) J Organomet Chem 507:275–277
4. Bunder W, Weiss E (1975) J Organomet Chem 92:65–68
5. Seiler P, Dunitz JD (1980) Acta Cryst Sect B 36:2255–2260
6. Fischer EO, Hofmann HP (1959) Chem Ber 92:482–486
7. Fischer EO, Grubert HZ (1956) Z Anorg Allg Chem 286:237–242
8. Resa I, Carmona E, Gutierrez-Puebla E, Monge A (2004) Science 305:1136–1138
9. Xie ZZ, Fang WH (2005) Chem Phys Lett 404:212–216
10. Xie YM, Schaefer HF III, Jemmis ED (2005) Chem Phys Lett 402:414–421
11. Luhl A, Nayek HP, Blechert S, Roesky PW (2011) Chem Commun 47:8280–8282
12. Schulz S, Schuchmann D, Westphal U, Bolte M (2009) Organometallics 28:1590–1592
13. Zhu H, Chen Y, Li S, Yang X, Liu Y (2011) Int J Hydrogen Energy 36:11810–11814
14. Janiak C, Schumann H (1991) Adv Organomet Chem 33:291–393
15. Li X, Kuznetsov AE, Zhang H-F, Boldyrev AI, Wang L-S (2001) Science 291:859–861
16. Mercero JM, Formoso E, Matxain JM, Eriksson LA, Ugalde JM (2006) Chem Eur J 12:4495–4502
17. Yang L-M, Ding Y-H, Sun C-C (2007) Chem Eur J 13:2546–2555
18. Boldyrev AI, Wang LS (2005) Chem Rev 105:3716–3757
19. Critchlow SC, Corbett JD (1984) Inorg Chem 23:770–774
20. Cisar A, Corbett JD (1977) Inorg Chem 16:2482–2487
21. Kuznetsov AE, Zhai H-J, Wang L-S, Boldyrev AI (2002) Inorg Chem 41:6062–6070
22. Li ZW, Wu WS, Li SH (2009) J Mol Struct (THEOCHEM) 908:73–78
23. Li ZW, Zhao CY, Chen LP (2007) J Theor Comput Chem 6:363–376
24. Wang C, Zhang X, Ge M, Li Q (2011) New J Chem 35:2527–2533
25. Becke AD (1993) J Chem Phys 98:5648–5652
26. Lee C, Yang W, Parr RG (1988) Phys Rev B 37:785–790
27. Becke AD (1988) Phys Rev A 38:3098–3100
28. Perdew JP (1986) Phys Rev B 33:8822–8824
29. McLean AD, Chandler GS (1980) J Chem Phys 72:5639–5648
30. Frisch MJ, Plple JA, Binkley JS (1984) J Chem Phys 80:3265–3269
31. Dolg M, Stoll H, Preuss H (1993) Theor Chim Acta 6:441–450

32. Bergner A, Dolg M, Kuechle W, Stoll H, Preuss H (1993) Mol Phys 6:1431–1441
33. Carpenter JE, Weinhold F (1988) J Mol Struct (THEOCHEM) 169:41–62
34. Foster JP, Weinhold FJ (1980) J Am Chem Soc 24:7211–7218
35. Reed AE, Weinstock RB, Weinhold F (1985) J Chem Phys 83:735–746
36. Reed AE, Curtiss LA, Weinhold F (1986) Chem Rev 6:899–926
37. Wolinski K, Hilton JF, Pulay P (1990) J Am Chem Soc 23:8251–8260
38. Schreckenbach G, Ziegler T (1995) J Phys Chem 2:606–611
39. Frisch MJ, Trucks GW, Schlegel HB, Scuseria GE, Robb MA, Cheeseman JR, Montgomery J A, Vreven T, Kudin KN, Burant JC, Millam JM, Iyengar SS, Tomasi J, Barone V, Cossi, Scalmani G, Rega N, Petersson GA, Nakatsuji H, Hada M, Ehara M, Toyota K, Fukuda R, Hasegawa J, Ishida M, Nakajima T, Honda Y, Kitao O, Nakai H, Klene M, Li X, Knox JE, Hratchian HP, Cross JB, Adamo C, Jaramillo J, Gomperts R, Stratmann RE, Yazyev O, Austin AJ, Cammi R, Pomelli C, Ochterski JW, Ayala PY, Morokuma K, Voth GA, Salvador P, Dannenberg JJ, Zakrzewski VG, Dapprich S, Daniels AD, Strain MC, Farkas O, Malick DK, Rabuck AD, Raghavachari K, Foresman JB, Ortiz JV, Cui Q, Baboul AG, Clifford S, Cioslowski J, Stefanov BB, Liu G, Liashenko A, Piskorz P, Komaromi I, Martin RL, Fox DJ, Keith T, Al-Laham MA, Peng CY, Nanayakkara A, Challacombe M, Gill PMW, Johnson B, Chen W, Wong MW, Gonzalez C, Pople JA (2003) Gaussian 03, Revision B.03. Gaussian Inc, Pittsburgh PA
40. te Velde G, Bickelhaupt FM, van Gisbergen SJA, Guerra CF, Baerends EJ, Snijders JG, Ziegler T (2001) J Comput Chem 22:931–967
41. Guerra CF, Snijders JG, te Velde G, Baerends EJ (1998) Theor Chem Acc 99:391–403
42. ADF2010, SCM, Theoretical Chemistry, Vrije Universiteit, Amsterdam, The Netherlands, http://www.scm.com
43. Chang C, Pelissier M, Durand Ph (1986) Phys Scr 34:394–404
44. Heully JL, Lindgren I, Lindroth E, Lundquist S, Martensson-Pendrill AM (1986) J Phys B 19:2799–2815
45. van Lenthe E, Baerends EJ, Snijders JG (1993) J Chem Phys 99:4597–4610
46. van Lenthe E, Baerends EJ, Snijders JG (1996) J Chem Phys 105:6505–6516
47. van Lenthe E, van Leeuwen R, Baerends EJ, Snijders JG (1996) Int J Quantum Chem 57:281–293
48. van Lenthe E, Ehlers AE, Baerends EJ (1999) J Chem Phys 110:8943–8953
49. Diefenbach A, Bickelhaupt FM, Frenking G (2000) J Am Chem Soc 122:6449–6458
50. Uddin J, Frenking G (2001) J Am Chem Soc 123:1683–1693
51. Pandey KK, Lein M, Frenking G (2003) J Am Chem Soc 125:1660–1668
52. Xu ZF, Xie YM, Feng WL, Schaefer HF (2003) J Phys Chem A 107:2716–2729
53. Uhl W (1988) Z Naturforsch B: Chem Sci 43b:1113–1118
54. Uhl W, Layh M, Hildenbrand T (1989) J Organomet Chem 364:289–300
55. Wang YZ, Robinson GH (2007) Organometallics 26:2–11
56. Rio Dd, Galindo A, Resa I, Carmona E (2005) Angew Chem Int Ed Engl 44:1244
57. Krygowski TM, Cyrañski MK, Czarnocki Z, Hafelinger G, Katritzky AR (2000) Tetrahedron 56:1783–1796
58. Cyran.ski MK, Krygowski TM, Katritzky AR, Schleyer PvR (2002) J Org Chem 4:1333–1338
59. Eluvathingal DJ, Boggavarapu K (1998) Inorg Chem 37:2110–2116
60. Krygowski TM (1993) J Chem Inf Comput Sci 33:70–78
61. Goldfuss B, Schleyer PvR, Schleyer PvR, Hampel F (1996) Organometallics 7:1755–1757
62. Glukhovtsev MJ (1997) Chem Educ 74:132–136
63. Schleyer PvR, Maerker C, Dransfeld A, Jiao HJ, van Eikema Hommes NJR (1996) J Am Chem Soc 26:6317–6318
64. Schleyer PvR, Najafian K, Kiran B, Jiao HJ (2000) Org Chem 65:426–431
65. Scheleyer PvR, Manoharan M, Wang ZX, Kiran B, Jiao HJ, Puchta R, van Eikema Hommes NJR (2001) Org Lett 3:2465–2468
66. Corminboeuf C, Heine T, Seifert G, Schleyer PvR, Weber J (2004) Phys Chem Chem Phys 6:273–276